Available online at www.sciencedirect.com
SCIENCE DIRECT®
Polymer 44 (2003) 5749–5758
polymer
www.elsevier.com/locate/polymer

Characterization of polyisoprene–clay nanocomposites prepared by solution blending

H.S. Jeon[a,*], J.K. Rameshwaram[a], G. Kim[b], D.H. Weinkauf[a]

[a]*Department of Petroleum and Chemical Engineering, New Mexico Institute of Mining and Technology, 801 Leroy Place, Socorro, NM 87801, USA*
[b]*Dow Corning Corporation, Midland, Michigan, MI 48686, USA*

Received 5 February 2003; received in revised form 16 May 2003; accepted 21 May 2003

Abstract

The effects of clay dispersion and the interactions between clays and polymer chains on the viscoelastic properties of polymer/clay nanocomposites are investigated using oscillatory shear rheology, X-ray diffraction (XRD), small-angle X-ray scattering (SAXS), and transmission electron microscopy (TEM). Four different montmorillonite silicates of natural clays, plasma-treated clays, and organically modified clays (OCs) have been used in this study. For the polyisoprene (PI)/clay nanocomposites, the exfoliation of the OC dispersed in the PI matrix is confirmed with XRD and SAXS although TEM images show both exfoliated and non-exfoliated nanoclay sheets. In contrast aggregation or intercalation is obtained for the other PI/clay composites studied here. Additionally, the effective maximum volume packing fraction of OC for the exfoliated nanocomposites is determined from the overlapping of dynamic viscosity at low frequency regime, in which the effective maximum volume packing fraction is larger than the percolation threshold determined from the storage modulus of the nanocomposites.

Keywords: Nanocomposites; Aspect ratio; Exfoliation

1. Introduction

In recent years, the nanocomposites which consist of polymer and nanoclays are of great interest for both scientific and practical industrial reasons due to their remarkable mechanical, thermal, chemical properties [1–11] as well as optical, electronic and magnetic applications [1,12,13]. The formation of nanoscale structure [14,15] and its response to applied shear are scientifically challenging and important to industry for processing. Rheological properties of nanostructured polymer/clay composites are strongly influenced by the morphology of these materials which depends on the clay dispersions (aggregation, intercalation, or exfoliation) in the polymer matrix. Rheological properties are therefore essential to relate the structure and properties of heterogeneous polymer/clay nanocomposites [1,2] or multiphase polymer blends [16–19], among others. Most experimental work reported in the literature has been focused on the mechanical or rheological properties of intercalated polymer/clay nanocomposites, in which pronounced viscoelastic or mechanical properties are typically observed [1–7]. However, the improvements in the viscoelastic or mechanical properties of polymer/clay nanocomposites have been limited up to approximately 2 orders of magnitude in most cases with adding a small amount of nanoclays (less than ~5%) due to the limited dispersion of layered silicates in polymer matrix. In order to develop and characterize exfoliated polymer/clay nanocomposites, we have studied a series of polyisoprene (PI)/clay composites with four different clays as a function of the clay weight fraction ($w = 0–0.09$).

In this paper, we use X-ray diffraction (XRD), small-angle X-ray scattering (SAXS), transmission electron microscopy (TEM), rheometry, and plasma-induced coating to study the structure and viscoelastic properties of aggregated, intercalated, and exfoliated PI/clay nanocomposites. In general, the morphology and viscoelastic properties of polymer/clay composites is affected by such things as processing methods, the composition and dispersion of clays, as well as the compatibility between polymer and clays.

* Corresponding author.

0032-3861/03/$ - see front matter © 2003 Elsevier Ltd. All rights reserved.
doi:10.1016/S0032-3861(03)00466-X

The purpose of the present work is to develop an exfoliated PI/clay nanocomposite and to study the effects of exfoliation and clay volume fraction, ϕ, on the viscoelastic properties of the PI/clay nanocomposites. The PI/clay nanocomposites may be used as a model system for polydienes/clay nanocomposites. The PI homopolymer is one of the most common polydienes that have been widely used in a synthetic rubber industry. We find exfoliation for the PI/OC nanocomposites, whereas conventional aggregation or intercalation is obtained for the other PI/clay composites studied in this work. We also determine the effective maximum volume packing fraction of the clay for the exfoliated PI/OC nanocomposites as the point of overlapping in the dynamic viscosity with increasing clay volume fraction. Additionally, the aspect ratio of the nanoclay sheets dispersed in the PI matrix is estimated using a modified Kriger's model for the viscosity of dispersion.

2. Experimental section

Organically modified commercial montmorillonite clay (Closite 10A, hereafter OC) and natural montmorillonite clay (Closite Na + , hereafter NC) were supplied from Southern Clay Products. The organically modified nanoclay (OC) with a charge exchange capacity of 1.25 mequiv/g was synthesized by a cationic exchange reaction between the layered silicate host and quaternary ammonium salt (methyl tallow bis-2-hydroxyethyl ammonium cation). The clay has a formula $M_x[Al_{4-x}Mg_x](Si_8)O_{20}(OH)_4$, where M is a monovalent charge compensating cation Na^+ in the interlayer and x is the degree of isomorphous substitution [3]. It was selected as a nanoparticle because of the high surface area (>750 m^2/g) and the large aspect ratio (100–500) when delaminated or exfoliated completely. Montmorillonite (MMT) is different from more commonly used clay minerals such as talc and mica, which are used as fillers in conventional polymer/filler composites. The organically modified MMT clays can be dispersed as individual nanoclay sheet (only $\sim$1 nm thickness and typical $\sim$400 nm in lateral dimensions) and the coherent stacks of layers ranging from $\sim$2 to $\sim$30 observed from TEM [20,23].

A commercial polyisoprene (PI) ($M_w \approx 40,000$; $M_w/M_n \approx 2$) was used as a matrix component in this study. PI was purchased from Aldrich Chemical and the microstructure was probed using ^{13}C nuclear magnetic resonance (NMR) and FTIR. PI is a statistical copolymer, composed of 1–4 and 3–4 isomers and has a mole fraction of 3–4 isomers equal to 0.07.

Surface treated clays are obtained by plasma polymerization. The plasma polymerization used for the coating of thin films by the influence of plasma on a monomer vapor and the subsequent deposition and polymerization of the excited species on the surface of the clays was carried out with a tumbling RF-plasma particle coating system. This process enables facile surface modification of small clay particles, which results in functionalized surface to promote interfacial compatibility with the PI molecules. The tumbling RF-plasma particle coating system used in this work was described in detail elsewhere [21]. The plasma reaction vessel (PRV) is inductively coupled to 13.56 MHz RF generator. The PRV is rotated to allow the random tumbling of the clays through the reaction plasma zone. The monomer flow rates are controlled with a monomer flow controller attached to the monomer feeding line. Also, the flask containing isoprene monomers is maintained at a constant temperature with thermostated water bath. With this system, isoprene monomers (Aldrich) are fed into a RF-plasma zone that contains mechanically fluidized (NC or OC) in a modified rotary vacuum system. In a typical coating procedure, the dried clay particles (NC or OC) to be treated are placed inside the reactor prior to evacuation. When the vessel pressure dropped to approximately 10^{-4} Torr, the reacting isoprene monomers was introduced at a constant flow rate and allowed to flow into the PRV.

The NC and OC particles plasma-treated with an isoprene monomer were labeled as PNC and POC, respectively. The plasma-polymerized materials thus formed on the surface of clay particles are quite different from conventional PI in both chemical and physical properties. However, it is expected that the coated films provide better compatibility or control of the particle interface in the PI/clay composites. By this technology, a thin film less than $\sim$100 nm in thickness with unique characteristics is formed on the clay surface exposed to the plasma. The details for the characterization of the plasma-treated clays are explored in a subsequent paper [22].

The PI/OC and PI/POC nanocomposites used in this study were prepared via solution blending [17]. We started with a dilute solution (mass fraction of $\sim$0.05 total polymer and clays) containing the appropriate amount of each component in a good solvent of toluene. The mixture was stirred at room temperature for about 14 h. The solvent was then evaporated under an atmosphere of flowing nitrogen gas, and the sample was dried in a vacuum oven at 50 °C for several days before measurements were performed. In contrast, the PI/NC and PI/PNC composites were prepared by simple mechanical mixing using a hand mixer since the NC and PNC particles are not dissolved in common solvents. The exact compositions and designation of the PI/clay composites used in this study are given in Table 1. The PI/NC, PI/PNC, PI/OC, and PI/POC composites are labeled as Ax, Bx, Cx, and Dx, respectively, where x is the weight percent of the clay in the composites.

XRD was used to determine basal d-spacing and performed using a Rigaku D/Max II X-ray diffractometer with Cu Kα radiation generated at 25 mA and 45 kV. Diffraction spectra were obtained over a 2θ range 2–10° in steps of 0.01° and counting times of 0.5 s at each angular position. SAXS was used for the structural analysis of the

Table 1
Characterization data of composites

Composites	Clays	w	ϕ^a	η_0' (Pa s)^b	G' (Pa)^b	G'' (Pa)^b
A5	NC	0.050	0.024	32	–	3.2
B5	PNC	0.051	0.024	33	–	3.3
C1	OC	0.010	0.005	34	0.07	3.8
C2	OC	0.020	0.011	58	0.35	5.8
C3	OC	0.031	0.015	640	81	64
C4	OC	0.040	0.019	12,700	1020	1400
C5	OC	0.050	0.024	49,000	20300	8200
C7	OC	0.071	0.034	265,000	34800	35100
C9	OC	0.092	0.045	289,000	63200	42500
D5	POC	0.050	0.024	110	0.90	11

[a] The polymer and clay densities used in the calculation of clay volume fraction are 0.883 and 1.90 at 50 °C, respectively.
[b] The dynamic zero shear viscosity and storage and loss moduli of composites were obtained at a $\omega = 0.1$ rad/s at 50 °C.

PI/clay nanocomposites on length scales from a few angstroms to a few micron using the UNM/Sandia SAXS instrument providing a wide q-range (0.003–7 nm^{-1}). The SAXS instrument used in this work was described in detail elsewhere [24].

The nanoclay distribution in polymer matrix were observed using JEOL 2000 FX at 200 KeV. In order to prepare thin nanocomposite films ($<\sim$100 nm thick), the solution of PI/OC mixture was deposited onto a salt substrate using a glass pipette and then spun off at $\sim$2000 rpm using a spin-coater. The film coated on a salt substrate was cut into squares and floated onto water. The thin specimens were collected on carbon coated Cu TEM grids from water. The images were taken using Gatan CCD camera attached under the TEM column with bright field TEM mode.

A PHYSICA UDS 200 Universal Dynamic Spectrometer was utilized in a parallel-plate geometry for oscillatory shear measurements, which were carried out with 25 mm diameter fixtures and a 0.4 ± 0.01 mm gap thickness. The temperature was controlled to within ±0.5 K, and all measurements were carried out at 50 °C under a nitrogen atmosphere to prevent any thermal degradation of the PI known to be sensitive to heat and air. In order to study the linear viscoelasticity, the oscillatory-shear measurements were performed on PI/clay composites at various frequencies (0.1 rad/s $\leq \omega \leq$ 100 rad/s) in a constant-strain mode using a small strain amplitude ($\gamma_0 < 0.02$) condition.

3. Results and discussion

3.1. Morphology: XRD, SAXS, and TEM

Fig. 1 shows the XRD curves of unmodified natural clay (NC), organically modified clay (OC), plasma-treated organoclay (POC), PI/PNC composite (B5), and PI/OC composite (C5) after annealing in vacuum oven at 50 °C.

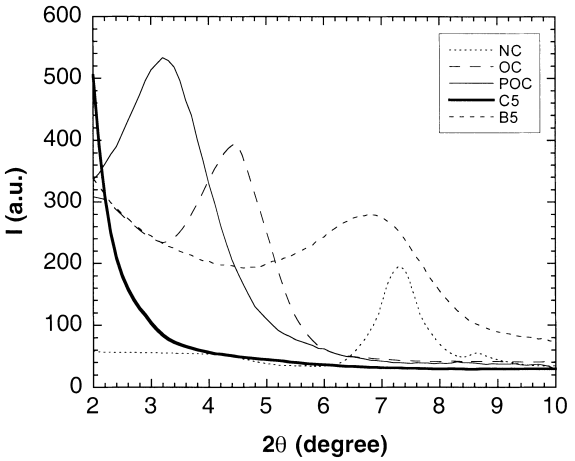

Fig. 1. X-ray diffraction (XRD) patterns for natural clay (NC), organically modified clay (OC), plasma-treated OC (POC), PI/PNC composite (B5), and PI/OC composite (C5). The basal d-spacing (d_{001}) for NC, OC, POC, and B5 are 12, 20, 27, and 13 Å, respectively. There are no peaks for the C5 nanocomposite, indicating that the basal d-spacing (d_{001}) of the nanoclays dispersed in the PI matrix is larger than ~4 nm.

The primary diffraction peaks at $2\theta = 7.35°$ (NC), 4.42° (OC), and 3.22° (POC) corresponds to a basal spacing (d_{001}) of 1.2, 2.0, and 2.7 nm, respectively. Also, the primary XRD peak for the B5 composite is located at $2\theta = 6.80°$ and much broader than that of the pure NC particle, suggesting that the coherent length of the silicate layer in the B5 composite is much larger than that of the NC particle. There are no peaks for the C5 nanocomposite in the range of $2\theta =$ 2–10°, indicating that the basal spacing (d_{001}) of the nanoclays in the C5 nanocomposite is larger than ~4 nm.

In order to confirm the exfoliation of the PI/OC (C-series) nanocomposites, we performed SAXS experiments on the all PI/OC nanocomposites studied here (C1 to C9). The typical scattering profile obtained from the C4 nanocomposite is shown in Fig. 2. It is evident that there are no peaks, indicating poor long-range order, in the wave

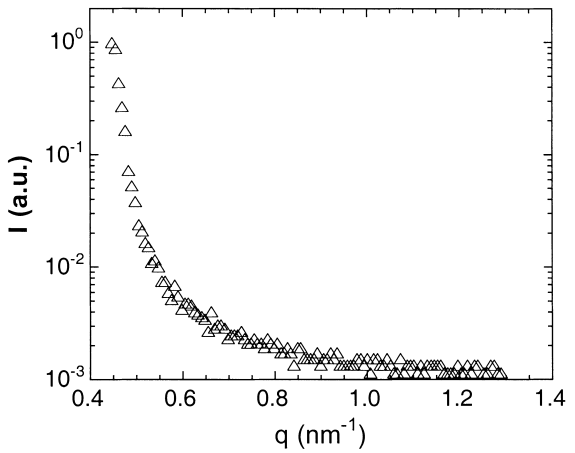

Fig. 2. Small-angle X-ray scattering (SAXS) profile for the C-series PI/OC nanocomposite (C4). The wave vector q values ranging from 0.45 to 1.29 nm^{-1} are corresponded to characteristic length scales ranging from 14 to 5 nm.

vector values ranging 0.44–1.92 nm^{-1} (corresponding to characteristic length scales, $2\pi/q$, ranging from 14.3 to 3.3 nm), where q is the wave vector ($q = (4\pi/\lambda)\sin(\theta/2)$), λ is the wavelength of X-ray, and θ is the scattering angle. This indicates that the nanocomposite was exfoliated with a gallery spacing, at least, greater than ~14 nm.

Clearly, the unmodified clays (hydrophilic) are incompatible with organophilic PI homopolymer molecules, and the narrow spacing (~1 nm) between layered nanoclay sheets imposes an entropic barrier for the penetration of the PI molecules into the narrow spacing. In contrast to the surface of the unmodified clays, the surface of the OCs has organophilicity (hydrophobic) although PI and OC do not have any specific functional groups. In our solution mixing process, the large polymer molecules penetrate into the spacing of layered nanoclay sheets in the organophilic environment and expand the spacing more than ~14 nm based on XRD and SAXS results, which is probably due to the immiscibility between PI and OC. It is interesting to note the results obtained from the polystyrene (PS)/OC (Closite-6A) and polyethylene (PE)/OC (Closite-6A) nanocomposites by Park et al. [25]. They reported that intercalation is obtained from the PS/OC nanocomposite due to the miscibility between PS and OC whereas exfoliation is obtained from the PE/OC nanocomposites due to the immiscibility between PE and OC. For the immiscible PS/OC nanocomposite, the attraction between PS chains and clay sheets might only lead to intercalation rather than exfoliation. In contrast, in the case of the immiscible PE/OC nanocomposite, the exfoliation might be obtained as the polymer chains try to retain its coil-like conformation and to gain entropy.

Fig. 3 shows the bright field TEM images of a typical exfoliated structure for the PI/OC nanocomposites at two different weight fractions of nanoclays: (a) C2 and (b) C4. It is clearly visible that the nanoclay sheets are randomly dispersed in the PI matrix. In addition to the formation of exfoliated nanoclay sheets, non-exfoliated nanoclay sheets are also observed. TEM images also show several large dark domains, which probably display the artifacts caused during the sample preparation. For the C2 and C4 nanocomposites (Fig. 3a and b), the nanoclay sheets dispersed in the PI matrix are shown from ~2 to ~14 nm in thickness [26]. The thickness of the dispersed nanoclay sheets seems to be larger than that of a single nanoclay sheet although the exfoliation of the nanocomposites was confirmed by means of XRD and SAXS. This may be due to that the nanoclay sheets shown as darker lines in the micrograph represent the projected thicknesses of the individual nanoclay sheets tilted from prismatic {110} or {010} surface and/or some of the nanoclays are not exfoliated completely.

We note that the TEM micrographs do not show any orientation of nanoclay sheets although the samples were prepared by spun casting at a speed ~2000 rpm. This can be understood with the aids of statistical mechanics of fluids of anisotropic particle dispersions. Onsager [27] showed that a

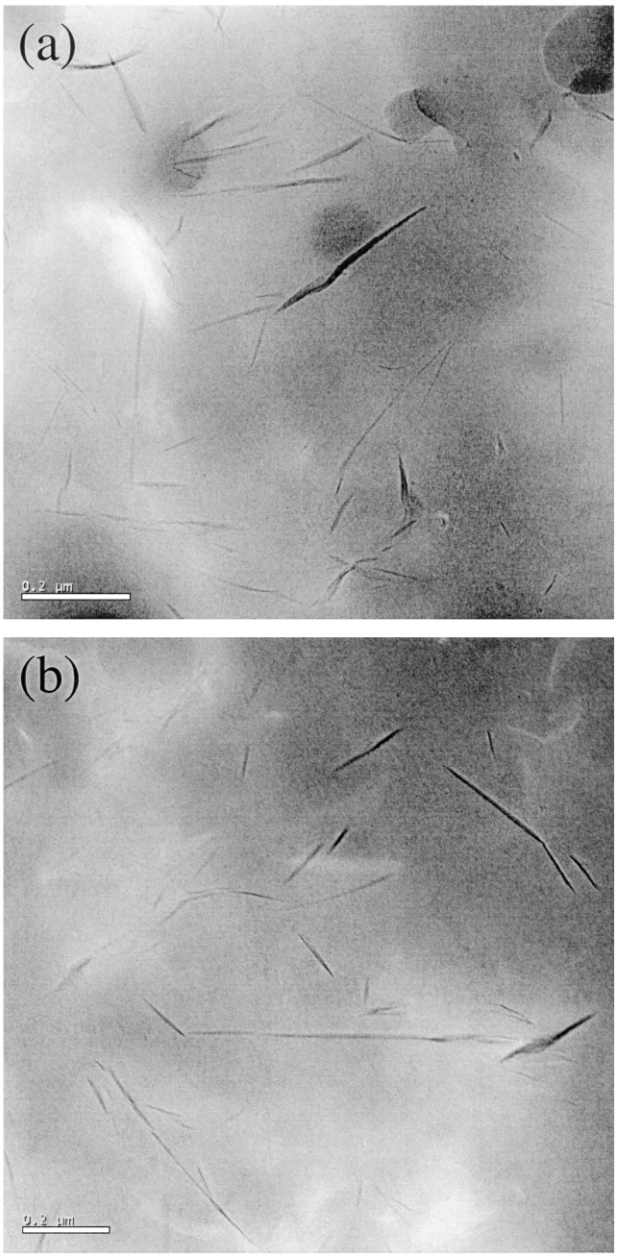

Fig. 3. Bright field TEM micrographs from the exfoliated C-series (PI/OC) nanocomposites: (a) C2; (b) C4. The scale bars in the TEM images (Fig. 3a and b) represent 200 nm.

distribution of platelets has an intrinsic tendency towards becoming ordered from disordered state spontaneously with increasing volume fraction (Φ) and aspect ratio (α). Dimarzio et al. [28] defined a crossover volume fraction (Φ_c) at which the equal amounts of the disordered and ordered phases are expected, and they found that $\Phi_c \approx 3.55/\alpha$. The crossover volume fraction (Φ_c) of the exfoliated PI/OC nanocomposites is predicted as 0.032 from the above relation with the average aspect ratio ($\alpha = 110$) of the nanoclay sheets dispersed in the PI matrix [23]. Therefore, the disordered phase of the dispersed nanoclay sheets may be more favorable for the nanoclay volume fractions up to

$\phi = 0.032$ or for the C1, C2, C3, C4, and C5 nanocomposites.

3.2. Linear viscoelasticity of PI/OC nanocomposites

At small strain amplitudes, the rheology measurements were carried out with minimal deformation of sample morphology. If the strain amplitude is sufficiently small, the ratio of stress to strain is only a function of time because the morphology slowly evolves with time. In order to determine the crossover from linear to non-linear viscoelasticity for the C-series nanocomposites, we performed a dynamic strain sweep at a constant frequency of 1 rad/s at 50 °C for a range of clay weight fractions ($w = 0.02–0.09$) as shown in Fig. 4. A linear viscoelastic response is evident from the constant values of storage modulus (G') as a function of the strain up to $\gamma_0 \approx 0.02$ at all clay weight fractions studied here. Therefore, the applied strain amplitude ($\gamma_0 \leq 0.01$) was within the linear viscoelastic regime.

3.3. Effects of clay surface modification

Fig. 5 shows the storage modulus (G') for PI homopolymer and PI/clay composites (A5, B5, C5, and D5) at a given weight fraction of clay ($w = 0.05$). It is clear that there are huge improvements of G' in the C5 nanocomposites with adding a small amount of nanoclays to the PI matrix. The improvement at a low frequency $\omega = 0.1$ rad/s is larger than ~6 orders of magnitude and the storage modulus exhibits frequency independence pseudo-solid like behaviors at lower frequencies ($\omega < 1$ rad/s). This is primarily due to the exfoliation of the nanoclay sheets that causes the formation of physical connectivity or percolated network of the nanoclay sheets at very small clay volume fractions because of their large aspect ratios ($\alpha >\sim 100$) and the high surface areas ($>750\ m^2/g$). Therefore, the perfect exfoliation of the nanoclays dispersed in polymer

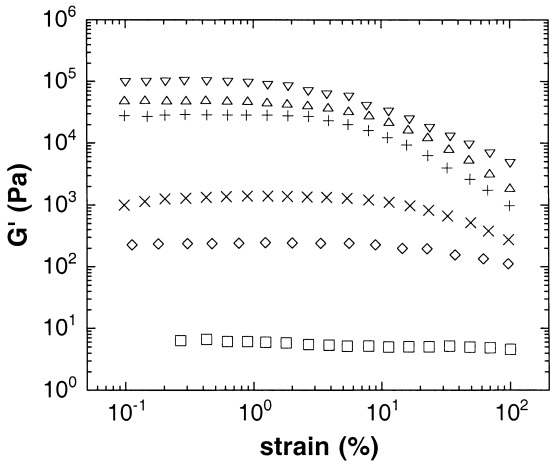

Fig. 4. Typical linear viscoelastic behaviors of the exfoliated PI/OC nanocomposites at a constant frequency of 1.0 rad/s. Symbols: C2 (square); C3 (diamond); C4 (cross); C5 (plus); C7 (triangle); C9 (reverse triangle).

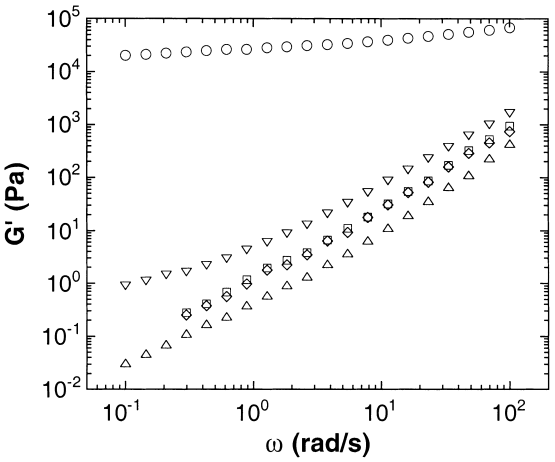

Fig. 5. Effects of clay particle treatment on dynamic storage modulus (G') for the PI/clay composites (A5, B5, C5, and D5) for a given clay weight fraction ($w = 0.05$). Symbols: PI (triangle); A5 (diamond); B5 (square); C5 (circle); D5 (reverse triangle).

matrix may exhibit highest improvements in viscoelastic properties for a given weight fraction of nanoclays since the perfect exfoliation provides the highest surface area and largest aspect ratio of the dispersed nanoclay sheets. The exfoliation of all C-series nanocomposites was confirmed with XRD and SAXS curves although the exfoliated and/or intercalated structures were observed in TEM images.

In contrast, for the storage moduli of the A5 and B5 composites, there are very small relative enhancement from the PI matrix because of incompatibility between organic polymer chains and inorganic clay particles. Also, there are negligible or no differences in G' between A5 and B5 although the B5 composite contains the plasma-treated clays (PNC). This is due to the agglomeration of the PNC particles in the PI matrix caused from the poor dispersion of clays although the compatibility between polymer and clays may enhanced from the plasma polymerized isoprene coating on the clay surface.

In order to confirm that the tremendous enhancements of G' in the PI/OC nanocomposites (C-series) is due to the exfoliation of nanoclays, we also measured the viscoelastic properties of the PI/POC composite (D5). POC is the surface treated OC via the plasma polymerization of isoprene monomers using the tumbling RF-plasma particle coating system. It is expected that the plasma polymerized PI coating will enhance compatibility or control of the particle interface in polymer/clay composites. Interestingly, the storage modulus of the D5 composites appears to be only ~10 times larger than that of the PI matrix at $\omega = 0.1$ rad/s, a relatively much smaller enhancements than that of the C5 nanocomposites. This suggests that the plasma-treated nanoclays (POC) are not exfoliated in the PI matrix, resulting in much lower enhancements in G', unlike in the case of the C-series nanocomposites.

Non-exfoliation in the D5 composites is probably due to the highly cross-linked plasma polymerized PI layer formed on the surface of aggregated clays by the plasma

polymerization of isoprene monomers. The plasma polymerized PI layer blocks the penetration or diffusion of the PI molecules ($R_g = 90$ Å) into the interlayer spacing of the layered silicates ($d_{001} = 20$ Å for OC) in the solution or melt state. The non-exfoliation of the D5 composite was confirmed by the TEM and optical microscopy in which, the clay particles were uniformly dispersed in the PI matrix with a length scale from ~0.5 to ~20 μm [22].

Fig. 6 shows the dynamic loss modulus (G'') of the PI/clay composites for a given weight fraction of clay ($w = 0.05$). There are also remarkable improvements in the loss modulus (G'') of the C5 nanocomposites and the relative improvement to the PI matrix is greater than ~3 orders of magnitude at a low frequency ($\omega = 0.1$ rad/s). The loss moduli of the A5 and B5 composites are virtually identical to those of the PI matrix at all frequencies (0.1–100 rad/s) studied here, whereas the storage moduli of these composites are slightly larger than that of the PI matrix (see Fig. 5). We thus note that G' is more sensitive than G'' to the dispersion of nanoclay sheets because the interfacial energy or compatibility between polymer and clays is much more sensitive to storage or elastic modulus than loss modulus. The loss modulus has been reported to be less sensitive to dispersion (intercalation or exfoliation) than storage modulus in various polymer/clay composites [1–4,6,7]. The loss modulus has been also shown to be either insensitive or weakly sensitive to the interfacial tension of phase separated or immiscible polymer blends [17,29–31].

3.4. Non-terminal zone behaviors of storage modulus

From the rheology measurements, we observe that the viscoelastic characteristics of the PI/OC nanocomposites are completely different from those of the PI homopolymer or conventional polymer-filler composite [2]. To examine the effects of clay weight fraction on the exfoliated PI/OC nanocomposites (C-series), we plot log G' vs. log ω for a range of clay weight fractions (0–0.09) as shown in Fig. 7. At low clay weight fractions ($w = 0.01$ and 0.02), the storage modulus shows a frequency dependence liquid-like behavior with the exponent (Γ) of the log G' vs. log ω plot to be 1.20 and 0.87 in the terminal regime, respectively. In contrast, at $w = 0.03$, the storage modulus jumps approximately 3 orders of magnitude from that of the PI matrix and the exponent is decreased up to 0.4 at the terminal regime. The experimental values of the terminal regime exponents for storage modulus vary between ~0.1 and ~1.5 for other intercalated or exfoliated polymer/clay composites [3,32,33]. The reported experimental values are ~0.5 for nylon-6/clay (5%) composites and ~0.3 for PS–PI block copolymer/clay (6.7%) composites [3], ~0.7 for polyamide-12/clay (4%) composites [32], and ~0.2 for poly(ϵ-caprolactone)/clay (3%) composites [33].

At higher clay weight fractions ($w > 0.04$), it is evident that there are tremendous improvements in the relative storage modulus ($G'_R = G'/G'_{PI}$) which is larger than approximately 6 orders of magnitude for $w > 0.05$ at low frequencies (Fig. 7), where G'_{PI} is the storage modulus of PI. We also observe a crossover from the frequency dependence liquid-like behavior to frequency independence pseudo-solid like behavior ($\Gamma \approx 0.1$) at low frequencies ($\omega < 0.5$ rad/s). The pseudo-solid like behavior is due to the formation of the physical connectivity or percolated network between the nanoclay sheets dispersed in the polymer matrix [1,4]. The exfoliated and/or intercalated polymer/clay nanocomposites may form a certain nanoscale structure. It is interesting that the C-series nanocomposites show the similar viscoelastic behaviors observed in microphase-separated block copolymers or liquid crystalline polymers having mesophase although the formation mechanism of the nanoscale structure in the polymer/clay nanocomposites is different to that of the block copolymers or the liquid crystalline polymers. Also, the non-terminal low frequency exponential values varying between ~0.3

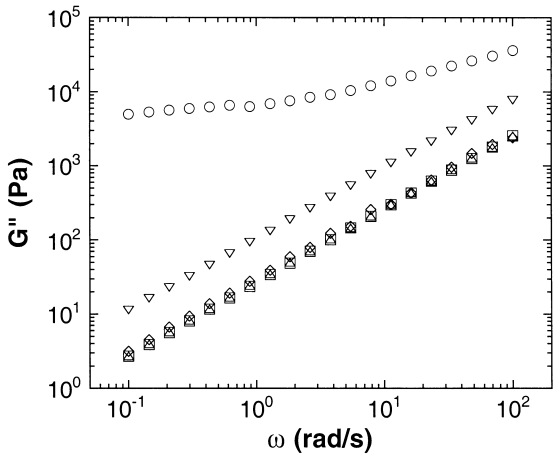

Fig. 6. Effects of clay particle treatment on dynamic loss modulus (G'') for the PI/clay composites (A5, B5, C5, and D5) for a given clay weight fraction ($w = 0.05$). Symbols: PI (triangle); A5 (diamond); B5 (square); C5 (circle); D5 (reverse triangle).

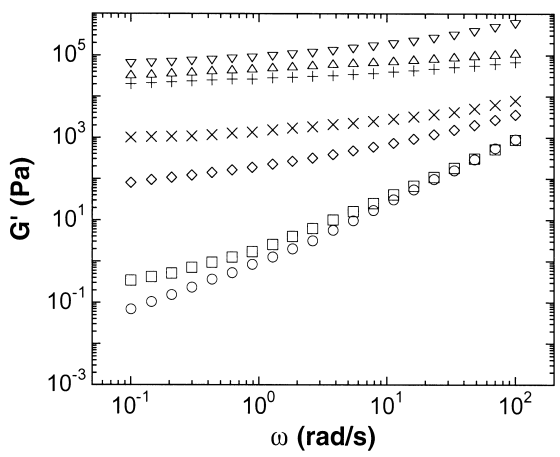

Fig. 7. Dynamic storage modulus (G') for the exfoliated PI/OC nanocomposites as a function of the organoclay (OC) weight fraction. Symbols: C1 (circle); C2 (square); C3 (diamond); C4 (cross); C5 (plus); C7 (triangle); C9 (reverse triangle).

and ~1.0 have been reported for polydispersed polymers [34], ordered diblock copolymers [35–37], liquid crystalline polymers [37], and phase separated polymer blends [17,38,39]. These examples suggest that the viscoelastic behaviors of the exfoliated C-series nanocomposite are similar to those of these systems.

Fig. 8 shows the experimental values of the terminal regime exponent (Γ) for G' for the different volume fractions of nanoclays. The exponent for the exfoliated C-series nanocomposites decreases smoothly as the clay volume fraction increases up to ~0.02, which is probably due to the increase of the interfacial area between nanoclays and polymer matrix or the enhancement in the physical interactions between nanoclay sheets. A plateau in the exponential value occurs at $\phi = 0.019$, which may be a critical volume fraction for percolation [40–42]. For $\phi > 0.019$, the constant value of Γ is shown because the dispersed nanoclay sheets may lead the formation of percolated network, which results in the pseudo-solid like behaviors at the low frequencies ($\omega < 0.5$ rad/s).

Fig. 9 shows the dynamic viscosity (η') of the exfoliated C-series nanocomposite for a range of clay weight fractions (0.01–0.09). The nanocomposite exhibits a Newtonian fluid behavior for $w \leq 0.02$ at all frequencies. In contrast the dynamic viscosity of the nanocomposite is characterized as shear-thinning fluids at all frequencies, and the slope (n) of log η' vs log ω can be expressed with a power-law equation ($\eta' \sim \omega^{-n}$). In the low frequency regime, the slope is 0.35 for C3, and increases up to 0.66 for C4. As the weight fraction of clay increases further up to 0.09, however, the slope in the low frequency regime exhibits a saturated value ($n \approx 0.83$) for C5, C7, and C9. In particular, there is a remarkable improvement in η' for C7, and the relative improvement ($\eta_r = \eta'/\eta'_0$) to the PI matrix is greater than ~5 orders of magnitude at $\omega = 0.1$ rad/s, where η'_0 is the zero-shear viscosity of the PI homopolymer.

Fig. 10 shows the relative dynamic viscosity ($\eta'_R = \eta'/\eta'_0$) of the PI/OC nanocomposite at a low frequency ($\omega = 0.1$ rad/s) as a function of the clay volume fraction. We also note that the viscosity is overlapped for $w \geq 0.07$ in the low frequency regime of $\omega < 0.4$ rad/s (Fig. 9). This indicates that the clay weight fraction is reached to a certain critical value above which the viscosity exhibits a very weak clay concentration-dependence or clay concentration-independence behavior in the terminal regime. Using the above information, we assign the point of discontinuity ($\phi \approx 0.032$) in the plot of log η_r vs. ϕ to viscosity percolation threshold (η_{PV}) [43] at which the viscosity approaches to a near plateau value for the exfoliated C-series nanocomposites indicated by an arrow (Fig. 10). The viscosity percolation threshold is then used as an approximation for the effective maximum packing fraction ($\phi_{m,e}$) of the C-series nanocomposite although $\phi_{m,e}$ is not a true maximum random packing volume fraction.

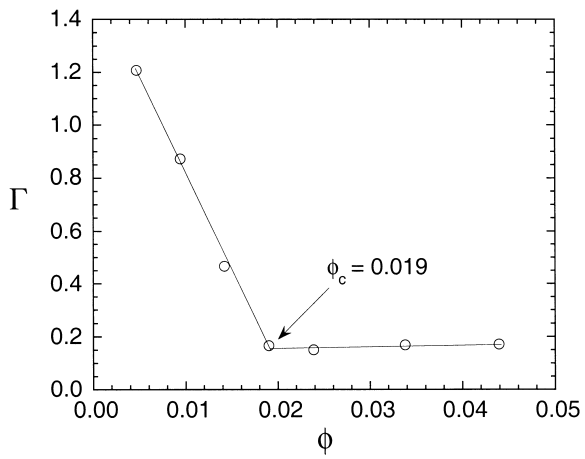

Fig. 8. Compositional dependence of the experimental exponent (Γ) of log $G' \sim$ log ω^{Γ} estimated for the exfoliated PI/OC nanocomposites (C-series).

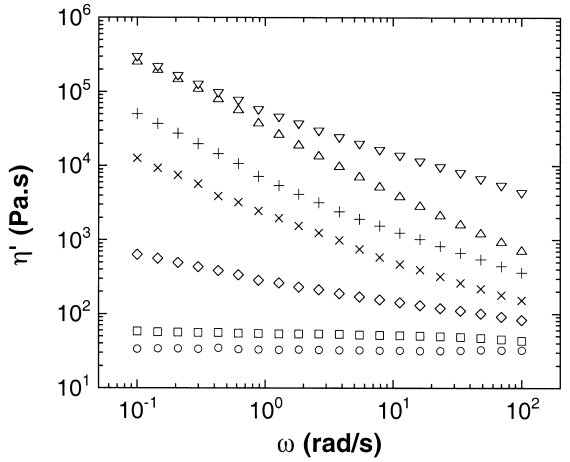

Fig. 9. Dynamic viscosity (η') for the PI homopolymer and exfoliated PI/OC nanocomposites (C-series) as a function of the organoclay (OC) weight fraction. Symbols: C1 (circle); C2 (square); C3 (diamond); C4 (cross); C5 (plus); C7 (triangle); C9 (reverse triangle).

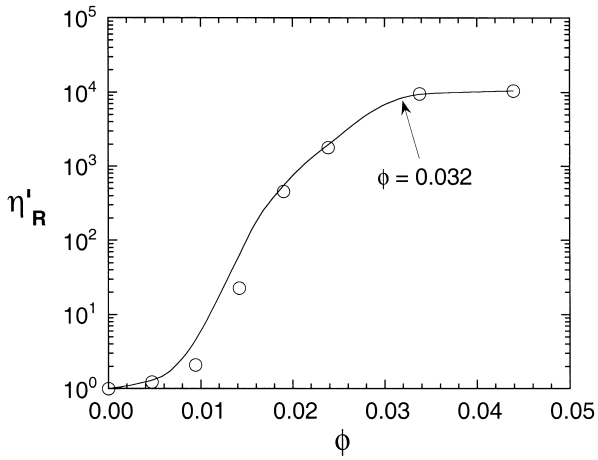

Fig. 10. Compositional dependence of the relative dynamic viscosity ratio ($\eta'_R = \eta'/\eta'_0$) for the exfoliated PI/OC nanocomposites (C-series). η' is the dynamic viscosity of the composite at a low frequency ($\omega = 0.1$ rad/s), η'_0 is the zero-shear viscosity of the PI homopolymer.

It is expected that the maximum packing volume fraction (ϕ_m) for the exfoliated PI/OC nanocomposites may be much larger than $\phi_{m,e}$. However, it was very difficult to prepare highly concentrated PI/clay nanocomposite samples ($\phi > \sim 0.1$) to determine the true maximum packing volume fraction for the exfoliated C-series nanocomposites. Also, it is difficult to determine ϕ_m for highly anisotropic particles because of possibly significant deviations from equilibrium particle configurations in modeling [43], and the model to predict the ϕ_m for the exfoliated polymer/clay nanocomposite is not available. In contrast, the correlation between ϕ_m and α is available as, $\phi_m = [2\ln(\alpha)]/\alpha$, for a cylindrical fiber over the range of $6.8 < \alpha < 143$ [43]. We may predict ϕ_m for the exfoliated PI/OC nanocomposites with an average aspect ratio (α) of nanoclay sheets if the above equation is valid for the exfoliated PI/clay system. The predicted maximum random packing volume fraction is 0.06–0.23 with the aspect ratio ($\alpha = 30$–190) obtained from TEM results, and the minimum value of ϕ_m is much larger than the value ($\phi_{m,e} \approx 0.032$) determined from the viscosity percolation threshold (Fig. 10).

The possible implication of the small value in the viscosity percolation threshold is probably due to the high aspect ratio of the nanoclay sheets in the exfoliated C-series nanocomposites. Moreover, the exfoliated nanoclay sheets have strong inter-silicates interactions or form highly percolated network when the clay volume fraction of the nanocomposites crosses to the viscosity percolation threshold (ϕ_{PV}). The effects of the silicate–silicate interactions and deformation of network structure under shear flow on the rheological properties of the exfoliated PI/clay composites are presented in a subsequent paper [44].

3.5. The aspect ratio of exfoliated nanoclays

A predictive model of the viscosity of filled polymers is an important issue for theory as well as for engineering applications. There have been reported so many models for the viscosity of dispersions as a function of the volume fraction and particle shape although the model for the viscosity of the dispersions containing highly anisotropic nanoparticles is not available. For the description of the influence of the nanoclays dispersion on the viscosity, we use the viscosity of a suspension as a model to study the relationships for the viscosity of the PI/clay nanocomposites as a function of the clay volume fraction and clay aspect ratio (α = width/thickness).

We used Eq. (1) to predict how the viscoelastic properties are affected with the dispersions or shapes of nanoclays although the equation is obtained from suspensions, in which particles and medium are immiscible. However, there are some similarities in viscoelastic behaviors between the exfoliated PI/OC nanocomposites and the suspensions having a high solid concentration [45]. To find a relationship between viscosity and concentration, we use a modified Krieger's empirical model equation [46] that gives a simple relative viscosity–concentration relationship with an intrinsic viscosity, [η]:

$$\eta_r = \left[1 - \frac{\phi}{\phi_{m,e}}\right]^{-[\eta]\phi_{m,e}} \quad (1)$$

In this equation, $\phi_{m,e}$ is the effective maximum packing volume fraction, which is about 0.637 for a random closest packing of spheres. For the application of this equation to the exfoliated C-series nanocomposites, we assume that the effective maximum packing volume fraction ($\phi_{m,e}$) is equal to the viscosity percolation threshold (ϕ_{PV}) although ϕ_{PV} is not a true maximum random packing volume fraction. The validation of this assumption is examined as the effective maximum packing volume fraction obtained from the C-series nanocomposite is applied to some viscosity–concentration models described in below to determine the aspect ratio of the nanoclay sheets dispersed in the polymer matrix. The aspect ratio determined from the model equations is then compared to the experimental value determined from TEM micrographs.

Fig. 11 shows the relative dynamic viscosity of the C-series nanocomposites at a given frequency ($\omega = 0.1$ rad/s) as a function of the clay volume fraction normalized with the effective maximum packing fraction ($\phi_{m,e}$) determined from the plot of log η_r vs ϕ. The solid curve is the fit for the Eq. (1) through the experimental data, and the intrinsic viscosity, [η], obtained from the best fit is 193.

For a laminar, the hydrodynamic motions of non-spherical particles are described as ellipsoids of revolution having their rotation axes properly oriented with respect to the flow direction. These ellipsoidal motions increase the viscosity of the system because those motions enhance the generation of viscous dissipation energy. Layered silicate

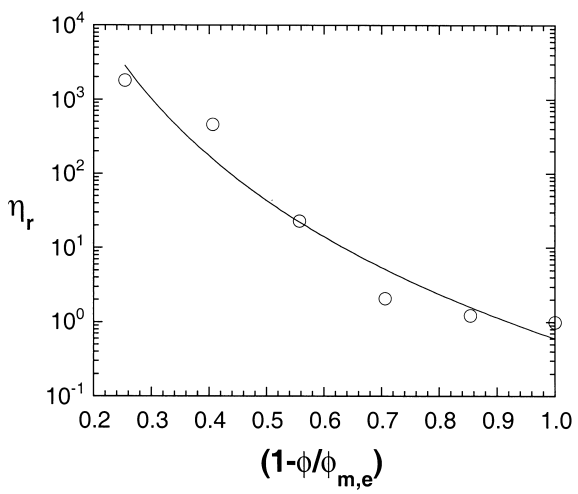

Fig. 11. The relative dynamic viscosity of the PI/OC (C-series) nanocomposites at a given frequency ($\omega = 0.1$ rad/s) as a function of the nanoclay volume fraction (ϕ) normalized with an effective maximum volume packing fraction ($\phi_{m,e}$) determined from the plot of log η_r vs ϕ. The solid curve is the fit for a modified Krieger's empirical model equation through the experimental data.

sheets commonly display thickness such as thin prismatic {010} and {110} surfaces in the intercalated or exfoliated nanocomposites. We observe that the nanoclay sheets preferentially display the prismatic surface for all the concentrations studied here ($w = 0.01 - 0.09$) instead of a large basal {001} surface. We thus use the Douglas and Garbochi approximation, Eq. (2), obtained from the Monte Carlo simulation of random dispersion [43], to determine the $[\eta]$ for oblate ellipsoids. They define the 'aspect ratio', $\beta = c/a$, as a measure of particle asymmetry, where c is the length of the minor symmetry axis of the ellipsoid and a is the asymmetry major axis of the ellipsoid. We thus note that $\beta > 1$ for prolate ellipsoids, $\beta = 1$ for sphere, and $\beta < 1$ for oblate ellipsoids (approximating nanoclay sheets).

$$[\eta] \approx \frac{1012 + 2904\beta - 1855\beta^{1.5} + 1604\beta^2 + 80.44\beta^3}{1497\beta + \beta^2} \quad (2)$$

We calculate the β value which satisfies $[\eta] \approx 193$ using the above equation. The average aspect ratio ($\alpha = 1/\beta$) of the nanoclay sheets for the exfoliated and/or intercalated PI/OC nanocomposites (C-series) was predicted as $\alpha \approx 282$. Although it might be argued that the model is good for the exfoliated polymer/clay nanocomposites, since it gives order-of-magnitude agreement with the average aspect ratio ($\alpha \approx 110$) obtained from TEM, a more detailed and quantitative theoretical treatment is clearly needed.

4. Conclusions

We have systematically investigated the structure and linear viscoelastic properties of the exfoliated and non-exfoliated PI/clay composites as a model system. We find exfoliation and/or intercalation for the PI/OC nanocomposites at a wide range of clay weight fractions ($w = 0.01 - 0.09$), whereas conventional aggregation (domain size $\sim$0.5–20 μm) or intercalation was obtained for the other PI/clay composites (A5, B5, and D5). In addition to the XRD profiles which do not show any peaks, TEM, SAXS, and rheology data provide further evidences for the exfoliation of the PI/OC nanocomposites.

We have also determined the effective maximum-packing volume fraction of clay for the exfoliated PI/clay nanocomposites based on the discontinuity in the dynamic shear viscosity as a function of clay volume fraction. The effective maximum-packing volume fraction ($\phi_{m,e} = 0.032$) is much larger than the percolation threshold ($\phi_p = 0.019$) determined from the critical clay volume fraction at which the storage modulus of the nanocomposites exhibits frequency independence pseudo-solid like behavior.

Additionally, we have predicted the average aspect ratio of the nanoclay sheets dispersed in the PI matrix from the models with the rheological and TEM data relating the intrinsic viscosity for dispersions of anisotropic particles to the aspect ratio of the dispersed particles. A reasonable order-of-magnitude agreement between experimental and theoretical values is obtained for the exfoliated and/or intercalated PI/clay nanocomposites. However, more theoretical and experimental work is needed to determine a true maximum-packing volume fraction and relate it to the aspect ratio of the exfoliated nanoclay sheets dispersed in the polymer matrix.

Acknowledgements

H.S.J. gratefully acknowledges the financial support of New Mexico Tech (Grant No. 11HX-11049). We thank Dr R. S. Seright (Petroleum Recovery Research Center) for his assistance during the rheology experiments. This work has been supported by a grant from the Department of Energy Materials Corridor Initiative.

References

[1] Pinnavaia TJ, Beall GW, Polymer–clay nanocomposites, New York: Wiley; 2001.
[2] Nakatani AI, Hjelm RP, Gerspacher M, Krishnamoorti R, Filled and Nanocomposite Polymer Materials Material Research Society Symposium, vol. 661. New York: MRS; 2001.
[3] Giannelis EP, Krishnamoorti R, Manias E. Adv Poly Sci 1999;138:107 and references therein.
[4] Krishnamoorti R, Ren J, Silva AS. J Chem Phys 2001;114:4968.
[5] LeBaron PC, Wang Z, Pinnavaia TJ. Appl Clay Sci 1999;15:11.
[6] Vaia RA, Jandt KD, Kramer EJ, Giannelis EP. Macromolecules 1995;28:8080.
[7] Messersmith PB, Giannelis EP. Chem Mater 1994;6:1719.
[8] Usuki A, Kojima Y, Kawasumi M, Okada A, Fukushima Y, Kurauchi T, Kamigaito O. J Mater Res 1993;8:1179.
[9] Hasegawa N, Kawasumi M, Kato M, Usuki A, Okada A. J Appl Polym Sci 1998;67:87.
[10] Burnside SD, Giannelis EP. Chem Mater 1995;7:1597.
[11] Vaia RA, Ishii H, Giannelis EP. Chem Mater 1993;5:1694.
[12] Godovsky DY. Adv Polym Sci 2000;153:163.
[13] Kumacheva E, Kalinina O, Lilge L. Adv Mater 1999;11:231.
[14] Collins PG, Zettl A, Bando H, Thess A, Smalley RE. Science 1997;278:100.
[15] Schlittler RR, Seo JW, Gimzewski JK, Durkan C, Saifullah MSM, Welland ME. Science 2001;292:1136.
[16] Han CD. Multiphase flow in polymer processing. New York: Academic Press; 1981.
[17] Jeon HS, Nakatani AI, Han CC, Colby RH. Macromolecules 2000;33:9732.
[18] Jeon HS, Hobbie EK. Phys Rev E 2001;63:61403.
[19] Jeon HS, Nakatani AI, Hobbie EK, Han CC. Langmuir 2001;17:3087.
[20] Manias E, Chen H, Krishnamoorti R, Genzer J, Kramer EJ, Gainnelis EP. Macromolecules 2000;33:7955.
[21] Russell SP, Weinkauf DH. Polymer 2001;42:2827.
[22] Jeon HS, Weinkauf DH. Unpublished results.
[23] The average value of aspect ratio was obtained from the aspect ratio of nanoclay sheets ($\alpha = 30 - 190$) estimated from TEM images for the exfoliated PI/OC nanocomposites (C5).
[24] Rieker TP, Hubbard PF. Rev Sci Instrum 1998;69:3504.
[25] Lim YT, Park OO. Rheol Acta 2001;40:200.
[26] The thickness range of the dispersed nanoclay sheets was obtained by examining full micrographs shown in Fig. 3a and b (6.5×6.5 μm^2).

[27] Onsager L. Ann New York Acad Sci 1949;51:627.
[28] DiMarzio EA, Yang AJ-M, Glotzer SC. J Res Nat Inst Stan Techn 1995;100:193.
[29] Pathak JA, Colby RH, Kamath SY, Kumar S, Stadler R. Macromolecules 1998;31:8988.
[30] Colby RH. Polymer 1989;30:1275.
[31] Zawada JA, Fuller GG, Colby RH, Fetters LJ, Roovers J. Macromolecules 1994;27:6851.
[32] Hoffmann B, Kressler J, Stoppelmann G, Friedrich Chr, Kim GM. Colloid Polym Sci 2000;278:629.
[33] Lepoittevin B, Devalckenaere M, Pantoustier N, Alexandre M, Kubies D, Calberg C, Jerome R, Dubois P. Polymer 2002;43:4017.
[34] Eckstein A, Friedrich Chr, Lobbrecht A, Spitz R, Mulhaupt R. Acta Polym 1997;48:41.
[35] Rosedale JH, Bates FS. Macromolecules 1990;23:2329.
[36] Rosedale JH, Bates FS, Almdal K, Mortensen K, Wignall GD. Macromolecules 1995;28:1429.
[37] Stuhn B, Mutter R, Albrecht T. Europhys Lett 1992;18:427.
[38] Nesaricar AR. Macromolecules 1995;28:7202.
[39] Mani S, Malone MF, Winter HH, Halary JL, Monnerie L. Macromolecules 1991;24:5451.
[40] de Gennes PG. In: Goldman AM, Wolf SA, editors. Percolation localization and superconductivity. NATO ASI Series B, Physics, vol. 109. New York: Plenum Press; 1984.
[41] Stauffer D. Introduction to percolation theory. London: Taylor and Francis; 1985.
[42] Grimmett G. Percolation. New York: Springer; 1989.
[43] Bicerano J, Douglas JF, Brune DA. Model for dispersion rheology. NIST: Polym Div 1998.
[44] Jeon HS, Rameshwaram JK. Effects of network deformation on the viscoelastic properties of polymer/clay nanocomposites. In preparation.
[45] Nielson LE, Polymer rheology, New York: Marcel Dekker; 1977.
[46] Krieger IM. Adv Colloid Interface Sci 1972;3:111.